

Original Research

## Quantum and Component Analysis of P3a and P3b from Auditory Single Trial ERPs Differentiates Borderline Personality Disorder from Schizophrenia

Dmitriy Melkonian<sup>\*</sup>, Anthony Korner, Russell Meares, Anthony Harris

Western Clinical School, 5 Fleet Street, North Parramatta, NSW, 2151, Australia; E-Mails: [dmitri.melkonyan@sydney.edu.au](mailto:dmitri.melkonyan@sydney.edu.au); [Anthony.Korner@health.nsw.gov.au](mailto:Anthony.Korner@health.nsw.gov.au); [russell.a.meares@gmail.com](mailto:russell.a.meares@gmail.com); [anthony.harris@sydney.edu.au](mailto:anthony.harris@sydney.edu.au)

\* **Correspondence:** Dmitriy Melkonian; E-Mail: [dmitri.melkonyan@sydney.edu.au](mailto:dmitri.melkonyan@sydney.edu.au)

**Academic Editor:** Severn B. Churn

**Special Issue:** [Synaptic Transmission](#)

*OBM Neurobiology*

2023, volume 7, issue 3

doi:10.21926/obm.neurobiol.2303174

**Received:** April 09, 2023

**Accepted:** July 04, 2023

**Published:** July 13, 2023

### Abstract

Traditional approaches to EEG modelling use the methods of classical physics to reconstruct scalp potentials in terms of explicit physical models of cortical neuron ensembles. The principal difficulty with such approaches is that the multiplicity of cellular processes, with an intricate array of deterministic and random influencing factors, prevents the creation of consistent biophysical parameter sets. An original, empirically testable solution has been achieved in our previous studies by a radical departure from the deterministic equations of classical physics to the probabilistic reasoning of quantum mechanics. This crucial step relocates the models of elementary bioelectric sources of EEG signals from the cellular to the molecular level where ions are considered as elementary sources of electricity. The rationale is that, despite dramatic differences in cellular machineries, statistical factors governed by the rules of the central limit theorem produce the EEG waveform as a statistical aggregate of the synchronized activity of multiple microscale sources. Based on these innovations, we introduce a method of comprehensive computerized analysis of event related potentials directly from single trial recordings. This method provides a universal model of single trial ERP



© 2023 by the author. This is an open access article distributed under the conditions of the [Creative Commons by Attribution License](#), which permits unrestricted use, distribution, and reproduction in any medium or format, provided the original work is correctly cited.

components in both frequency and time domains. For the first time, this tool provides effective quantification of all significant cognitive components in single trial ERPs and represents a viable alternative to the traditional method of averaging. We demonstrate the clinical significance of the additional information provided by the new method, using ERP data from patients with borderline personality disorder and schizophrenia. Referring to the P300 as an important objective marker of psychiatric disorders, we show that the new method reliably identifies P3a and P3b as the major components of the P3. The diagnostic significance of differentiating the P3a and P3b components of P3 is that it provides an objective electrophysiological measure that distinguishes borderline personality disorder from schizophrenia.

### **Keywords**

Single trial ERP; P3a; P3b; borderline personality disorder; schizophrenia; quantum analysis; birth and death process; fragmentary decomposition; transient deterministic chaos

## **1. Introduction**

The recording of human electroencephalogram (EEG) by means of electrodes on the scalp is one of the most widely used functional tests of neural function with excellent temporal resolution. The exquisite sensitivity of EEG to changes in mental activity has been documented in numerous studies. A fundamental criterion used to link electrophysiological and cognitive variables is a concomitant variation of neurophysiological and psychological processes. In consequence, the key to understanding of the information processing context of EEG signals is provided by detection of the changes in ongoing EEG activity which is time-locked to a particular cognitive event.

The EEG peaking waveform which frequently appears at specific time intervals linked to the application of a cognitive stimulus is known as an event-related potential (ERP).

An overlap of ERP components with the ongoing oscillations of the EEG is a factor which obscures the morphology of ERPs. Therefore, signal extraction methods are absolutely essential in ERP analyses.

The most common method is ensemble averaging which consists in summation of a series of EEG epochs (trials), each of which is time-locked to the event of interest. The basic assumption of the method is that pertinent EEG fragments are the summands of two sources: (i) the ERPs which are constant over trials, (ii) random constituents that are not time-locked to the event. The first assumption asserts that identical time-locked ERPs are expected in response to repeated cognitive events. However, there is a great deal of experimental evidence that this assumption is an oversimplification which disregards the fact that ERP composition consists of multiple components, each of which is subject to trial-to-trial variability governed by different probabilistic laws.

The fact that the same event can elicit somewhat different signals has been evident for a few decades and is clearly seen from the following general psychophysiological definition of endogenous ERP components: "The components must be nonobligatory responses to stimuli. The same physical stimulus, presented to the same subjects, sometimes will and sometimes will not elicit the component" [1].

Consequently, the conventional ensemble average would not necessarily correspond to any of the individual single-trial responses. This means that without an account of stochastic factors, ensemble averaging creates ambiguity with respect to the analysis and interpretation of ERPs. An account of the diversity of single trial ERPs provides more information related to changes of cognitive state in response to the stimulus.

A lot of effort has been invested in inventing methods of estimating ERPs directly from single trials. The difficulty in developing this approach relates to the basic mechanisms that underlie the generation of the EEG signal.

It is generally accepted that EEG signals are distant manifestations of synchronized activities in populations of cortical neurons. The processes involved are complex and their interpretation rests mainly on an empirical understanding. The development of EEG models has been widely researched and, until recently, has been approached using the methods of classical physics [2, 3]. The major proposition is that cortical neurons are the elementary microscale sources of the EEG waveforms. Such an approach assumes that, in principle, EEG dynamics can be deduced from physical models of neuronal ensembles [2]. On these grounds, the membrane potentials produced in some way by the cortical neurons appear as the “building blocks”, from which the EEG waveforms are composed. In particular, the proposition that EEG waves are constituted primarily by the postsynaptic potentials of cortical neurons is widely accepted.

However, because electrical activity associated with a single neuron is small, it is only possible, using scalp electrodes, to detect the integrated activity of many neurons. The creation of a corresponding model using the methods of the classical theory of electromagnetism would need to be supported by the parameters of all participating neurons. Significant difficulties are created by the anatomical complications posed by the multiplicity of cellular elements, along with an insufficient knowledge of their morphological details and functional relationships. This leads to an intractably large number of degrees of freedom and prevents a unique determination of mass effect. Under conditions of such uncertainty no single model of EEG dynamics has yet achieved the goal of integrating the wide variety of parameters of separate neurons or neuronal ensembles into the dynamics of EEG waveforms. In a review of the state of art, Michael Cohen notes that, “surprisingly little is known about how the activity in neural circuits produces the various EEG features” [4].

A radically different approach to the treatment of mass potentials, the category of signals to which the EEG and single trial ERP belong, has been achieved by a departure from the deterministic equations of classical physics to the probabilistic formalism of quantum mechanics [5]. The crucial step is relocation of the microscale origins of the macroscale potentials from a cellular to a molecular level. Instead of the continuous time membrane potentials implemented in previous theories, the key role for elementary cortical sources of electricity is attributed to ions, positively and negatively charged particles, the size and stochasticity of which conform to quantum mechanics. A major outcome supported by the probabilistic formalism of quantum mechanics and the central limit theorem is a link between the global scale mass potential and the underlying microscale events [5].

The quantum theory of mass potentials has been subsequently elaborated in several ways for EEG and single trial ERP analyses [6]. A crucial outcome of this novel methodology is its ability to create remarkably accurate models of single trial ERPs and effectively disclose the multiplicity of

ERP components. This is particularly important for detection and measurement of positive ERP waves of approximately 300 ms peak latency whose average is known as P3 or P300.

The P3 has been broadly studied in psychiatric disorders and is widely accepted as the most important marker of cognitive functions [1]. Conventional utilization of average P3 ignores the complex component composition of this component, specifically the P3a and P3b sub-components, reflecting contributions of various generators to the ERPs.

The significant clinical value of additional information provided by single trial ERP analysis and identification of the P3a and P3b components has been demonstrated in the study of cortical arousal in children and adolescents with functional neurological symptoms [7]. It was shown that specific changes of the P3a and P3b amplitudes disclose pathology of the coordination between frontal and posterior generators of brain electrical activity.

The importance of the account of component composition of P3 has been demonstrated in the study of single trial auditory ERPs in BPD patients [8]. The P3a, which depends on the circuitry having prefrontal connections, was significantly larger than in normal controls and similar in amplitude to young adolescents. In addition, the P3a failed to habituate, which suggested a failure of pre-frontally mediated inhibitory mechanisms.

It is widely acknowledged that prefrontal deficiencies are also evident in schizophrenia.

Both BPD and schizophrenia are disorders of integration [9]. Though the form of disintegration in the two conditions differs functionally, the pattern of symptoms can sometimes overlap. For example, both may experience hallucinations [10]. Misdiagnosed patients may risk being exposed to the wrong treatment.

The possibility to improve diagnostics using electrophysiological tools is supported by the fact that reduction in amplitude of the average P3 from the standard auditory oddball paradigm is one of the most replicable biological observations of schizophrenia, present regardless of medication status [11].

A similar abnormality in BPD has been reported in a comparative study of patients with BPD and schizophrenia, where the authors report, "The ERP abnormalities found in patients with BPD are indistinguishable from those found in patients with schizophrenia" [12]. However, the methodology of average ERPs used in the study ignores the complex component composition of P3, specifically its P3a and P3b sub-components, reflecting contributions from various generators.

These facts indicate a need, unfulfilled by traditional methodologies of average ERPs, to enhance the comparative analysis of BPD and schizophrenia by reliable identification of the dynamics of single trial P3a and P3b as well as the trial-to-trial variability of these components.

## **2. Methods and Materials**

### **2.1 Quantum Analysis**

It is generally assumed that EEGs are distant manifestations of electrical phenomena occurring on the microscopic scale, consisting of cortical ensembles of multiple excitable cells immersed in interstitial fluid. This activity can be recorded on the surface of the scalp because the tissue that lies between the source and the scalp acts as a volume-conductor.

The elementary sources of the EEG are ions, both positively and negatively charged particles the passages of which across membranes are governed by probabilistic rules [13].

The contribution of a single ion to the changes in electrical potential differences between various locations in the extracellular space is vanishingly small. This means that measurable changes of the extracellular potentials (field potentials) are produced by the mass effects of multiple elementary sources [14]. Two requirements must be fulfilled for this integration to occur: a) the cells must be closely located and comprise an ensemble with functional connectivity of its elements; (b) the activation of the cells must be synchronized or at least closely related in timing. We call such a cellular ensemble a local cortical generator (LCG).

Previous models of elementary sources of EEG waveforms considered the continuous time membrane potentials as constituents of scalp potentials. As detailed elsewhere [6], the major innovative aspect of the methodology which we call the quantum EEG (QEEG) is that the elementary cortical sources of electricity are attributed to ions, positively and negatively charged particles, the size and stochasticity of which conform to quantum mechanics.

QEEG refers to the fact that the interior and exterior of a cell from a LCG, be it a neuron or a glial cell, are both varieties of saline solution (water with ions dissolved in it) separated by membranes. Considering the membrane as a border, the tissue can be divided into an extracellular and intracellular space. To a good approximation, the extracellular space can be considered independent of the intracellular space, because its boundaries, the cell membranes, have high resistances (several  $k\Omega \cdot \text{cm}^2$ ), compared with the resistance of the extracellular space ( $\sim 200 \Omega \cdot \text{cm}$ ). An important factor is that, within the range of frequencies of physiological interest (0-1 kHz), the capacitive, inductive, magnetic, and propagative effects of bioelectrical phenomena in the extracellular space can be neglected [15]. Thus, the extracellular space may be regarded with reasonable accuracy as a resistive medium.

The populations of ions separated by membranes are illustrated by the schematic diagram in Figure 1. The whole-colored cloud in the left panel shows the LCG, i.e. a cell ensemble which is capable of producing changes in field potentials.

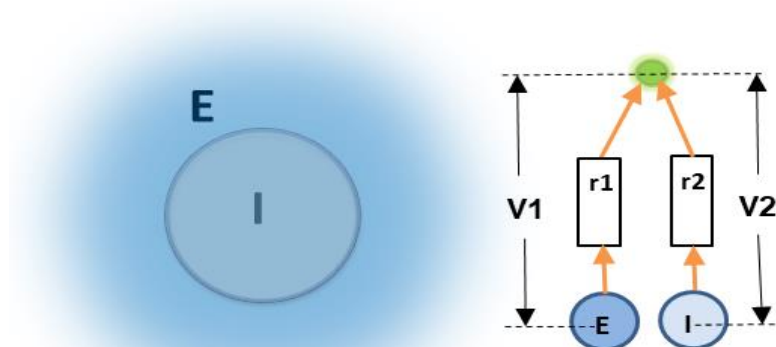


**Figure 1** Schematic diagram of LCG and its E and I compartments.

The ions inside the cells of the LCG are considered as contents of the interior compartment **I**, shown by the circle. The ions from the exterior of the cells composing the LCG are considered as the contents of the external compartment **E**.

Since the **I** and **E** compartments are separated by membranes working as insulators, they are shown in the right panel of Figure 1 as isolated, separate sources of electricity, **E** and **I**, respectively.

The exchange of particles between the compartments is regarded as a birth and death process (BDP). An increase of the compartment size by a unit represents birth, .as a decrease by a unit represents death. A probabilistic theory of similar transport processes developing in chemical synapses has been introduced in the previous papers [16, 17]. We use this theory for introduction of the rules which govern the transmembrane ion transport.

To evaluate the contribution of ions from the E and I compartments to generation of field potentials, the reference is made to the potential differences  $V_1$  and  $V_2$  between the compartments and electrical ground shown in the top of the right panel as a small green circle. This element is associated with the cortical electrode.

In fact, it is not the voltages themselves but electric currents flowing in the extracellular space, that define the influence of the LCG on field potentials. To a good approximation these currents are defined as:

$$i_1 = V_1/r_1 \text{ and } i_2 = V_2/r_2.$$

Here  $r_1$  is the resistance of the extracellular space, while  $r_2 = r_1 + r_M$ , where  $r_M$  is the resistance of the membrane. The internal structure of such systems may be almost impossible to delineate precisely. The power of the QEEG methodology is that probabilistic methods deal with statistical properties and do not demand detailed descriptions of specific circuits. The supporting basis of QEEG, which is not particularly concerned with the morphology of the LCG, is the fact that

$$r_M \gg r_1.$$

Accordingly,  $i_1 \gg i_2$ , which means that currents produced by the extracellular sources are remarkably larger than the currents from intracellular sources. Separating the interior of the cells from the extracellular space, membranes prevent the ions located inside the neurons from producing measurable changes of the current flow in the extracellular space. In contrast, the cumulative effects of the charges of ions released from the cells during synchronized activation of cellular ensembles may influence the dynamics of the global scale EEG.

On these grounds the global scale potential is linked to the net charge of positive and negative ions released from LCG cells and existing in the extracellular space. Such an ensemble of ions was termed STION (STochastic IONS) in an earlier paper [6].

Physically, the aggregate of particles considered as a STION represents a thin cloud of cations and anions spread over the outer surfaces of membranes of the cells composing the LCG. Functionally, the ensemble of particles composing a STION represents the sum of the primary and secondary particle populations, the behavior of which is governed by the following rules.

**Rule 1.** *During resting conditions, transmembrane ion transport is balanced. The behavior of both particle populations develops as simple BDP with constant birth and death rates*

$$\lambda = \mu = \eta/\sigma^2.$$

**Rule 2.** *After activation at  $t = t_0$  by the triggering event the transient behavior of the primary particle population develops as a non-homogenous BDP with a constant rate of birth*

$$\lambda_p = \eta/\sigma^2,$$

and time-dependent rate of death

$$\mu_p(t) = (t - t_0)/\sigma^2.$$

**Rule 3.** After activation at  $t = t_0$  by the triggering event, the transient behavior of the secondary particle population develops as a non-homogenous death process with a time-dependent rate of death

$$\mu_s(t) = (t - t_0 + \eta)/\sigma^2 = \mu_p(t) + \lambda_p.$$

Unique tools for reconstruction of the time courses of particle populations predicted by these rules are numerical simulations which deal with the number of particles  $X_N(t)$  composing the net charge, and the numbers of particles in the primary and secondary populations,  $X_P(t)$  and  $X_S(t)$ , respectively [6]. The results of a typical simulation [6], reproduced in Figure 2, extend over the time interval from -10 to 70 ms with  $t = 0$  corresponding to the instant at which the transient condition starts. As an initial condition, an equal size of 50 particles was prescribed for both populations. The parameters were  $\sigma = 13.3$  ms and  $\eta = 26.2$  ms.

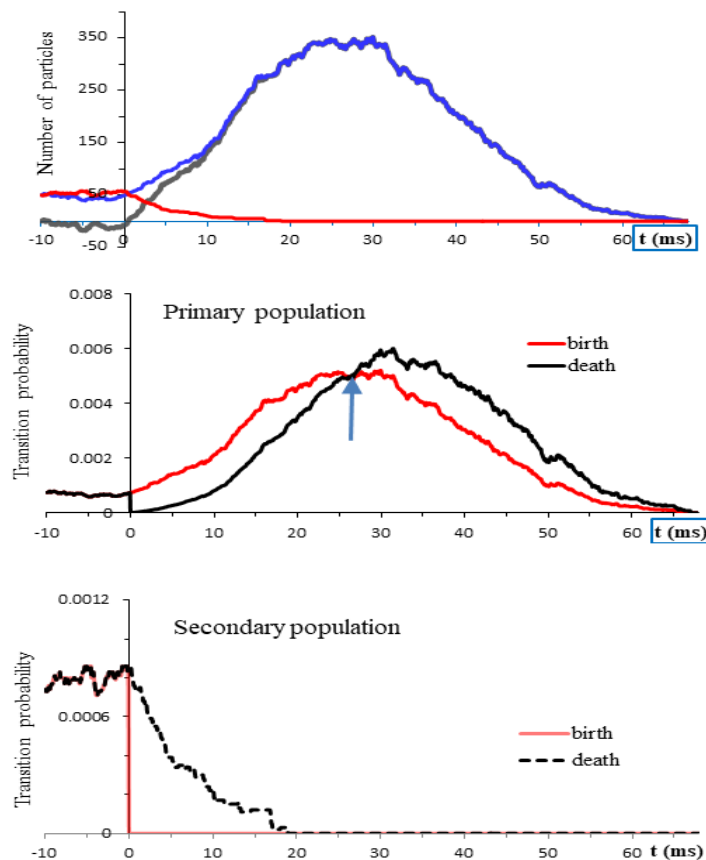


**Figure 2** Numerical reconstructions of the temporal evolution of particle populations in a typical trial. The resting conditions computed from -10 ms are turned at  $t = 0$  to the transient conditions. The blue, red, and black lines in the top panel show the functions  $X_P(t)$ ,  $X_S(t)$  and  $X_N(t)$ . The time courses of the underlying transition probabilities are shown in the middle and bottom panels.

During resting conditions (interval from -10 ms to  $t = 0$ ) the transport of particles between the primary and secondary populations is balanced. A rapid change of the net charge induced by onset of the transient condition is due almost entirely to the change of the birth and death rates in the primary particle population.

The size of the primary population is governed by the complex interplay of the birth and death transition probabilities. The onset of transient conditions gives rise to both probabilities. Initially, from  $t = 0$  to the time instant indicated in the middle panel of Figure 2 by the arrow, the birth probability prevails over the death probability. At this stage nearly a tenfold increase of the size of the primary population occurs. After the peak, the death probabilities take a progressively larger share. As a result, the size of the primary population declines and returns to the initial conditions. The effect of the transients in the secondary particle population on the net charge is minor and brief compared with the primary population.

A general picture emerging from quantum analysis is that under resting conditions the STION develops as a stationary process. The triggering event induces specific changes of particle movements, the summary effects of which determine EEG component waveforms.

The essential outcome of quantum analysis is a description of the behavior of multi-particle systems of the STION with many degrees of freedom in terms of global scale EEG components with few “macroscopic” degrees of freedom. The reference is made to the central limit theorem as a tool that defines the limiting behavior of ensembles of random variables [18]. A specific aspect of the methodology of the QEEG is that the limiting distributions are estimated using both time and frequency domain variables [6].

The time domain solution is given by

$$\psi(t) = (\sigma\sqrt{2\pi})^{-1} [\psi_P(t) - \psi_S(t)] \quad (1)$$

where,

$$\psi_P(t) = \exp[-(t - \eta)^2/2\sigma^2],$$

$$\psi_S(t) = \exp[-(t + \eta)^2/2\sigma^2].$$

The equation (1) is consistent with the wave function in a general form of the d'Alembert's solution to the wave equation [19]. In this context  $\psi(t)$  is the sum of a right traveling wave  $\psi_P(t)$  and a left traveling wave  $\psi_S(t)$ . A crucial difference is that the d'Alembert's wave function is defined on an infinite time scale while  $\psi(t)$  is zero at  $t < 0$ . In the context of this specific feature the  $\psi(t)$  is called a *half-wave function* (HWF). The two terms from which the  $\psi(t)$  is composed are considered as products of the *primary particle population* associated with  $\psi_P(t)$  and the *secondary particle population* associated with  $\psi_S(t)$ . These functions are illustrated in Figure 3.

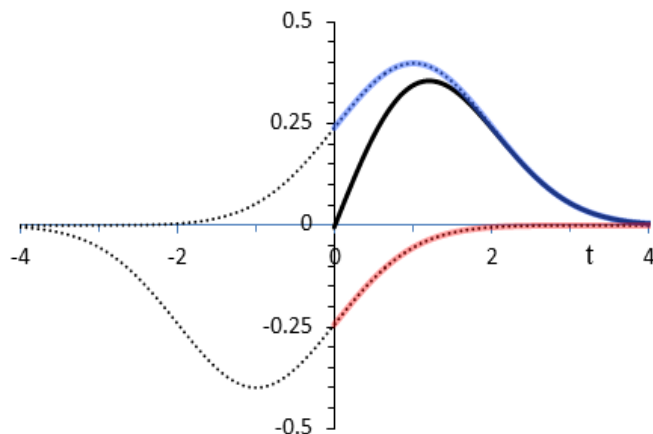


**Figure 3** Given  $\sigma = \eta = 1$ , the black, blue, and red solid lines show  $\psi(t)$ ,  $\psi_P(t)$ , and  $\psi_S(t)$ , respectively. The dotted lines are Gaussian functions which indicate that  $\psi_P(t)$  and  $\psi_S(t)$  are fragments of the two shifted curves of normal distributions.

## 2.2 Component Analysis

There is general agreement that the EEG is a complex signal composed from multiple components produced by activation of various cortical processors. ERP components are conventionally defined as the peaks which are labelled according to the polarity (N-negative, P-positive) and the peak latency (L). Thus, N1 (abbreviation of N100) refers to a negative peak with L of about 100 ms, and P3 (abbreviation of P300) refers to a positive peak with L of approximately 300 ms.

A universal model of single trial ERP component is described by equation 1 [20]. The fact that  $\eta$  and  $\sigma$ , defined as the parameters of macroscale HWF, also govern the molecular events creates a bridge between the EEG and underlying micro-scale phenomena. Using a model component in the form of HWF, the model of an EEG segment with “N” components is given by the following sum of weighted HWFs

$$h(t) = \sum_{k=1}^N z_k(t) \tag{2}$$

where  $z_k(t) = g_k \cdot \psi_k(t - \tau_{k-1})$ .

The index “k” in this formula labels different HWFs with corresponding  $\sigma_k$  and  $\eta_k$  parameters.  $g_k$  is the weighting coefficient and  $\tau_k$  is the time instant from which the development of the corresponding component starts.

The specifics of the QEEG methodology is that the estimation of the parameters of each term in the right-hand side of equation (2) are performed by the method of high resolution fragmentary decomposition (HRFD) which consists of two stages: the spectral analysis and parametrization [21, 22].

### 2.2.1 Spectral Analysis

The spectral analysis starts from adaptive segmentation. Considering the EEG as a time function  $v(t)$ , the procedure deals with the series of samples  $v_m = v(t_m)$  at regular, discrete time points  $t_m = m\Delta$ , where  $\Delta$  is the sampling interval. The segmentation points are estimated as zero-crossings and points of global and local minima of  $|v(t)|$ . By ordering the segmentation points, both zero-crossings and minimums, as consecutive time points, the sequence of the segmentation points  $\tau_0, \dots, \tau_k, \dots, \tau_K$  is formed. The EEG segment between sequential segmentation points is called an empirical half wave (EHW). Given a segment of the length  $T_k = \tau_k - \tau_{k-1}$  between the points  $\tau_{k-1}$  and  $\tau_k$  ( $i = 1, \dots, K$ ), the EHW is defined as

$$w_k(t) = \begin{cases} v(t + \tau_{k-1}) & \text{if } 0 \leq t \leq T_i, \\ 0 & \text{otherwise.} \end{cases}$$

In the interval from 0 to  $T_i$  this function reproduces the EEG fragment between the segmentation points  $\tau_{k-1}$  and  $\tau_k$ .

The frequency domain counterpart of  $w(t)$ , the complex spectrum, is defined by the exponential finite Fourier transform

$$W(i\omega) = W_C(\omega) - iW_S(\omega) = \int_0^T w(t)\exp(-i\omega t) dt, \quad (3)$$

where  $\omega = 2\pi f$ ,  $f$  is frequency and  $i = \sqrt{-1}$ . Since manipulations with various EHWs are universal, the number of EHWs is omitted,

Because  $w(t)$  is an empirical entity, the calculations of such integrals are performed numerically. A serious computational problem is that readily available techniques of digital spectral analysis, such as the Fast Fourier transform, is devoted to the estimation of the power spectrum. It is not suited for short-term spectral decompositions. As an adequate tool the SBF algorithm is employed, a novel version of the Filon-type methods that provide maximum precision in the estimation of trigonometric integral [23]. The SBF algorithms deals with continuous Fourier spectra instead of the discrete spectra utilized by conventional spectral analysis. Of crucial importance here is that dealing with EEG segments of different lengths, the SBF algorithm does not demand windowing, zero-padding or other techniques for reducing the errors produced by the spectral leakage.

### 2.2.2 Parametrization

The choice of time-frequency analysis as a tool for adequate estimation of the EEG model in the form of equation 2 has been supported by the finding on an empirical basis of an appropriate approximant of the frequency domain images of EHWs in the form of a universal complex spectrum

$$G(i\omega) = Y(\omega) \cdot \exp[-i\varphi(\omega)], \quad (4)$$

where,

$$Y(\omega) = \exp[-(\sigma\omega)^2/2], \quad (5)$$

$$\varphi(\omega) = \eta\omega. \tag{6}$$

$Y(\omega)$  and  $\varphi(\omega)$  are considered as the models of the amplitude spectrum and the phase function of the system associated with HWF. The amplitude spectrum and frequency are normalized to express these entities in dimensionless units.

The normalized amplitude spectrum is defined as

$$Y^*(\omega) = Y(\omega)/Y(\omega_0),$$

where  $Y(\omega)$  is the computed amplitude spectrum and  $\omega_0$  is a sufficiently small value of angular frequency selected to satisfy the condition:  $Y(\omega_0) \approx Y(0)$ . The red line at the middle panel of Figure 4 illustrates a typical normalized amplitude spectrum. It was calculated from the EHW depicted at the top of the figure. The red line shows the fit of the theoretical amplitude spectrum (5) to the empirical  $Y^*(\omega)$ .

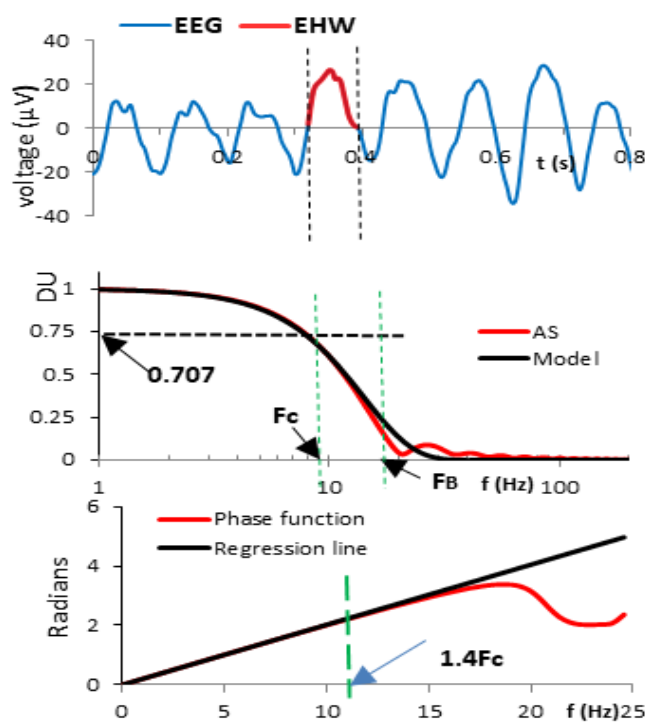


**Figure 4** Top panel: the blue line shows 800 ms segment of a typical EEG, the vertical dotted lines delineate the EHW. The red lines in the middle and bottom panels show the normalized amplitude spectrum and the phase function calculated from selected EHW. The black line in the middle panel shows the Gaussian template at position defined by the best fit. The black line in the bottom panel is a regression line which illustrates the typical linearity of the phase function in the frequency range from  $F_0$  to  $1.4 \cdot F_c$ .

An important factor supporting the fitting procedure is that  $Y^*(\omega)$  can be considered as the frequency response of a low pass filter, the conventional parameter of which is the cut-off frequency  $F_c$ . At this frequency the attenuation of the amplitude spectrum drops by 3 dB, i.e.  $Y^*(\omega_c) = 1/\sqrt{2}$ , where  $\omega_c = 2 \pi F_c$ .

The cut-off frequency serves as a basis unit, the use of which defines the relative frequency as  $\gamma = \omega/\omega_c$ .

Using the dimensionless amplitude and frequency, the empirical amplitude spectrum is defined in relative units as  $Z(\gamma) = Y^*(\omega_c\gamma)$ . The corresponding model is the Gaussian spectrum

$$G(\gamma) = \exp(-\gamma^2). \quad (7)$$

Note that  $Z(\gamma) = G(\gamma)$  at  $\gamma = 1$ , the relative frequency which corresponds to  $f = F_c$ .

In most cases combining  $Z(\gamma)$  and  $G(\gamma)$  at  $\gamma = 1$  provides a close agreement between these entities. In a systematic manner the comparison is performed more fully by a fitting procedure, the goal of which is to find the best match of analytical  $G(\gamma)$  to empirical  $Z(\gamma)$ .

Starting from the frequency  $F_0 = \omega_0/2\pi$ , the accuracy of the fit is evaluated by the value of the mean square error between  $Z(\gamma)$  and  $G(\gamma)$ . The position of the best fit defines the boundary frequency  $F_B$ . Numerous trials with various EHWs revealed that typically the template from the best fit virtually coincides with the amplitude spectrum in the range of standard frequencies from 0 to 1. At  $\gamma > 1$  the errors increase with increases in frequency.

The larger  $F_B$  is in comparison with  $F_0$ , the more accurate the Gaussian model of the amplitude spectrum. For assessing goodness of fit, the dimensionless extension ratio  $\varepsilon = F_B/F_c$  is used. The fit in the middle panel of Figure 4 gives a visual idea of how the  $F_c$  and  $F_B$  are related.

Calculations of  $\sigma$  are followed by the estimation of phase functions. It was found that the initial part of the phase function  $\phi(\omega)$  shows consistency with a simple linear model

$$\varphi(\omega) = \xi\omega$$

where  $\xi$  is a parameter.

Numerous calculated linear fits indicate that deviation from linearity can be neglected over the frequency range from 0 to  $1.4 \cdot F_c$ . A typical result is illustrated in the bottom panel of Figure 4. Thus, the estimation of  $\eta$  is reduced to the calculation of the linear regression line using  $\phi(f)$  samples from  $f = f_0$  to  $f = 1.4 \cdot F_c$ . The slope of the regression line  $\xi$  serves as the estimate of the parameter  $\eta$ .

Given particular  $w_k(t)$  from equation 2, the estimated  $\sigma$  and  $\eta$  define the corresponding  $\psi_k(t)$  term. Using these data, the weighting coefficients are derived from the following interpolation conditions separately applied to each pair of EHW and HWF:

$$a_k \cdot \psi_k(P_k) = w_k(P_k),$$

where  $P_k$  is the peak latency of the  $k$ th EHW. Consequently,

$$a_k = w_k(P_k)/\psi_k(P_k).$$

Thus, the peak latencies and amplitudes of the model are equalized to the peak latencies and amplitudes of EHW.

### 2.2.3 Single Trial Analysis

Creation of adequate models of EEG segments by the methodology of QEEG is supported by an original method of single trial analysis of ERPs [20]. The procedure starts from the extraction of EEG

segments time-locked to the target stimuli. Given a particular EEG channel with a digitally stored data set, for each of the first 40 target stimuli, standard 2 s EEG segments were extracted, from 1 s pre-stimulus to 1 s post-stimulus. The segments were digitally filtered (moving window averaging) to remove irrelevant low (<0.5 Hz) and high (>50 Hz) frequency components. For each channel these procedures provided a time series with 500 samples  $v[nT]$ , where  $n$  takes values  $-250, \dots, 0, \dots, 249$  ( $n = 0$  is the time of the target stimulus onset) and  $T = 0.004$  s.

The application of the high-resolution fragmentary decomposition (HRFD) [22] provides a model of a single trial in the form of equation 2. The parameters  $\sigma_i$  and  $\eta_i$  of each identified HWF are transformed to conventional parameters:  $A_i = 0.356\sigma_i$ -peak amplitude and  $L = t_i + 1.2\eta_i$  - peak latency. Physically,  $1.2\eta$  is the rise time, the time interval during which the component increases from zero to its maximum value. This measure becomes available due to the shape estimate (parameter  $\eta$ ) provided by the HRFD technique.

An extended system of parameter windows has been developed for identification of conventional late ERP components N1(00), P2(00), N2(00), P3a and P3b. Given  $L$  - peak latency,  $A$  - peak amplitude and  $\eta$  - shape constant as the major parameters, the identified HWF is qualified as a meaningful ERP component if it satisfies the conditions specified by the following windows:

Condition 1:  $L_1 \leq L < L_2$  (latency window),

Condition 2:  $A_1 \leq A < A_2$  (amplitude window),

Condition 3:  $\rho_1 \leq \rho < \rho_2$ . (shape window).

The  $L_1$  and  $L_2$  (ms) parameters of the latency windows were as follows: P50 from, -20 to 75, N1 from, -80 to 120, P2 from, -160 to 220, N2 from, -180 to 235, P3a from, -240 to 299, P3b from, -300 to 360. The parameters of the shape windows for all components were:  $\rho_1 = 8$  ms and  $\rho_2 = 50$  ms. The  $A_1$  and  $A_2$  ( $\mu\text{V}$ ) parameters of the amplitude windows were -45 and -2 for negative and 2 and 45 for positive components, respectively.

#### 2.2.4 Averaging Procedures

Contemporary understanding of endogenous potentials is mostly based on the visual examination and quantitative analysis of average ERPs. The traditional method of averaging assumes that single trial recordings consist of identical time-locked ERPs and random constituents that are not time-locked to the event. However, it is widely accepted that this assumption is an oversimplification which discounts the reality that ERP composition is made up of multiple components, each of which is subject to trial-to-trial variability which may be governed by different factors. Elucidation of the nature of these components requires explicit analysis of various ensembles of identified single trial ERP components.

Our methodology of HRFD identifies ERP components in each single trial and creates a model of the single trial ERP in the form of equation 2. This solution provides a basis for a novel method of averaging which we call selective component averaging (SCA). The averaging is applied to identified HWFs which satisfy conditions 1-3 for the component of interest. The SCA of selected components is defined by the sum

$$u^D(t) = \frac{1}{M_i} \sum_{i=1}^{M_i} e_i^D(t - \tau_{Di}), \quad (12)$$

where the symbol “D” stands for the name of the component,  $M_i$  is the number of selected HWFs and  $\tau_{Di}$  is the time instant from which the HWF starts. The sum of models defined by this equation is called a synthetic average. For example, synthetic average of the late positive complex consisting of the P3a and P3b has the form,

$$u^{LPC}(t) = \frac{1}{M_a} \sum_{i=1}^{M_a} e_i^{P3a}(t - \tau_{P3ai}) + \frac{1}{M_b} \sum_{i=1}^{M_b} e_i^{P3b}(t - \tau_{P3bi}),$$

where  $M_a$  and  $M_b$  are the numbers of  $P3_a$  and  $P3_b$  components delivered through SCA.

SCA improves the accuracy of average waveforms because it selects the trials with identified (i.e. meaningful) components and ignores trials with missing components.

To account for missing responses, we introduce a novel parameter called an elicitation rate (ER). This parameter takes into account the actual number  $A$  of the trials in which the component was defined:  $A = T - M$  where  $T$  is the total number of single trials and  $M$  is the number of the trials with missing components. The ER is defined as  $P_E = A/T$ . This parameter is the probability of the elicitation of a defined component in a single trial.

### 2.3 Subjects

Three groups of age- and sex-matched subjects have been investigated in this analysis, drawn from 2 earlier studies [8, 24]:

17 unmedicated patients with BPD, 17 patients with schizophrenia and 17 healthy controls. The BPD patients (4 males and 13 females; range = 20-44 years; mean age = 31.6) came from an ongoing program for the treatment and evaluation of BPD patients. The diagnosis was made by two independent raters (psychiatrist and psychologist), according to DSM-III-R criteria in a diagnostic interview that included the Diagnostic Interview for Borderline Patients. Patients were free of medication for at least 30 days at the time of the study.

The schizophrenia patients (4 males and 13 females; range = 20-44 years; mean age = 31.6) were drawn from a larger sample recruited from hospitals and community centres in Sydney. All participants had been diagnosed with schizophrenia for at least 4 years. The diagnosis was made through concordance between the case file diagnosis and diagnosis based on CIDI Section G, according to DSM-IV criteria [25].

The control group included 17 matched subjects (4 males and 13 females; mean age = 34.3, sd = 8.6, range = 20-47 years).

Exclusion criteria for all groups were a recent history of substance abuse, past history of substance dependence, intellectual disability or other neurological disorders including epilepsy and head injury [assessed using Section M from the Composite International Diagnostic Interview (CIDI) and the Westmead Hospital Clinical Information Base questionnaire (WHCIB)]. Subjects were asked to refrain from smoking or drinking caffeine for three hours prior to the recording session. Ethics approval was obtained for the original projects from the Western Sydney Area Health Service Ethics Committee [8, 24]. Written consent was obtained from all subjects prior to testing in accordance with National Health and Medical Research Council guidelines.

## 2.4 Procedure

Subjects were seated in a sound and light attenuated room. Each subject had their eyes open and was instructed to fixate on a colored dot in the center of a screen, in order to minimize eye movements. An electrode cap [26] was used to acquire data from Fz, F3, F4, F7, F8, Cz, C3, C4, T3, T4, Pz, P3, P4, O1, and O2 scalp sites. Linked earlobes served as the reference. Horizontal eye movement potentials were recorded using two electrodes, placed 1 cm lateral to the outer canthus of each eye. Vertical eye movement potentials were recorded using two electrodes placed on the middle of the supraorbital and infraorbital regions of the left eye. All electrode impedances were less than or equal to 5 k $\Omega$ . A 32-channel continuous acquisition system with DC amplifiers was employed. EEG and EOG channels had a range of  $\pm 13.75$  mV and a resolution of 0.42  $\mu$ V.

ERP data were collected according to a standard auditory "oddball" paradigm. Stereo headphones conveyed regular tones of 1000 Hz at an interval of 1.3 seconds to both ears. Eighty-five percent of these were 1000 Hz tones which the subjects were instructed not to respond to (task irrelevant). The other 15% were target (task relevant) tones of 1500 Hz. These high tones (targets) were intermixed with the lower (background) tones in a pseudorandom sequence, with the constraints that two target tones were never presented in succession, and the number of background tones between targets was always an odd number between 1 and 11 inclusive. Total tone duration was 60 ms, including a 10 ms rise time and 10 ms fall time.

The subjects were instructed to respond to target tones by pressing two reaction-time buttons, as fast and accurately as possible, with the middle finger of each hand (to counterbalance motor effects). Speed and accuracy were emphasized equally in the task instructions. All tones were presented at 60 dB above the subject's auditory threshold (determined prior to recording).

The experiments for each subject consisted of a 4 min session during which the stimuli application times were recorded simultaneously and continuously with the 32-channel EEG and 2-channel electro-oculogram (EOG).

A low pass filter was applied to the analogue voltages prior to digitization. The cutoff of this filter was 50 Hz, with the attenuation being 40 dB per decade above 50 Hz. In addition, a 50 Hz notch filter was applied to eliminate 50 Hz AC mains power supply interference.

Filtered voltages were continuously digitized at 250 Hz and digitally stored with the markers of the instants of stimuli applications.

## 2.5 Statistical Analyses

### 2.5.1 Kolmogorov Smirnov Test

The procedures of parameter estimation described above define the frequency range of the best fit of the theoretical amplitude spectrum to the empirical amplitude spectrum of EHW from  $F_0$  to  $F_B$ . Comparison of different fits is enabled by the dimensionless extension ratio  $\varepsilon = F_B/F_C$ . Given the samples of  $\varepsilon$  in the form of two different ensembles,  $\mathcal{E}_1 = \{\varepsilon_1^1, \dots, \varepsilon_n^1, \dots, \varepsilon_N^1\}$  and  $\mathcal{E}_2 = \{\varepsilon_1^2, \dots, \varepsilon_k^2, \dots, \varepsilon_K^2\}$ , the Kolmogorov-Smirnov one and two sample tests are used in order to decide whether  $\mathcal{E}_1$  and  $\mathcal{E}_2$  are produced by the same or different distributions. Each of the data sets  $\mathcal{E}_1$  and  $\mathcal{E}_2$  is converted to a cumulative frequency distribution. The test is based on evaluation of the maximum vertical deviation  $D$  between the cumulative frequency distributions. The null

hypothesis that the two distributions are the same is rejected if the value of D exceeds the critical value defined by the tables of D statistics.

### 3. Results

The analysis of various EEG and ERP recordings in both the patient and control groups and the results of many numerical experiments provide ample evidence that half-wave function  $\psi(t)$ , emerging as the macroscopic scale effect from synchronized chaotic ion movements on the microscopic scale, can be regarded as a universal building block from which these signals are composed.

Figure 5 illustrates typical results of the application of QEEG methodology for creation of an explicit model of a single trial ERP composed of multiple components. The dynamics of the EEG signal shown in the upper panel on the interval from -100 ms to 500 ms is affected at  $t = 0$  by the application of the target auditory stimulus. This event produces a single trial ERP which represents at  $t > 0$  a specific succession of positive and negative waveform deflections, the 6 species of which have been identified as conventional P50, N1, P2, N2, P3a and P3b late component ERPs.

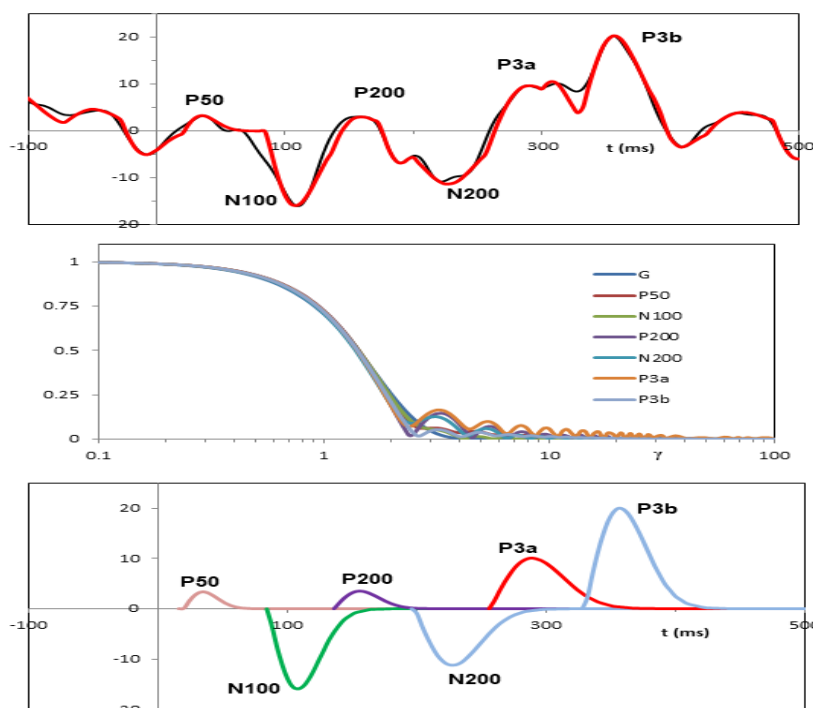


**Figure 5** A typical model of single trial ERP from Cz recording site with its components identified by the HRFD.

Normalized amplitude spectra of these components are shown in the middle panel. The line “G” is the normalized amplitude spectrum. It appears as a limiting form of the empirical spectra.

The sum of all identified HWFs is a model single trial ERP which is shown in the top panel by the red line. The models of separate ERP components are shown in the bottom panel.

A remarkably accurate match of the models to empirical curves is typical for the identification procedures of the HRFD). The key observation is a mutual coincidence of empirical amplitude spectra in a wide range of the relative frequency  $\gamma$  from 0.1 to 100.

An appealing feature of these results is that models of various EEG and ERP waveforms are obtained without requiring knowledge of the details of the underlying cellular and molecular systems. This paradigm is consistent with the phenomenon known in quantum theories as *universality*. Conceptually, *universality* means that, despite a profound diversity of complex dynamic systems observed in nature, particularly biology, their topology may have universal characteristics regarded as universal objects. Our methodology for the first time identifies such universal elements directly from the dynamics of EEG and single trial ERP signals.

The universality indicates the stochastic nature of the mechanisms which produce the macro-scale EEG waveforms and ERP components. The composition of the HWF as a sum of two shifted Gaussian functions suggests that the normal distribution governs transitions from the micro- to macro-scales.

The Kolmogorov-Smirnov tests were employed to examine this conclusion (a null hypothesis that the corresponding statistical regularities follow the normal distribution). This test has the advantage of making no assumption about the distribution of the samples, since it is non-parametric and distribution free.

The  $\varepsilon$  (dimensionless extension ratio =  $F_B/F_C$ ) has been selected as an adequate parameter for these tests because this single measure is sufficient to evaluate the fit of results.

Typical results illustrated in Figure 6 were obtained using single trial recordings from Fz, Cz and Pz cortical sites [6]. For each location the values of  $\varepsilon$  were collected from 20 different identified EHWs. The EHW was accepted as eligible for testing the D-statistics if the number of EHW's samples was  $\geq 8$ .

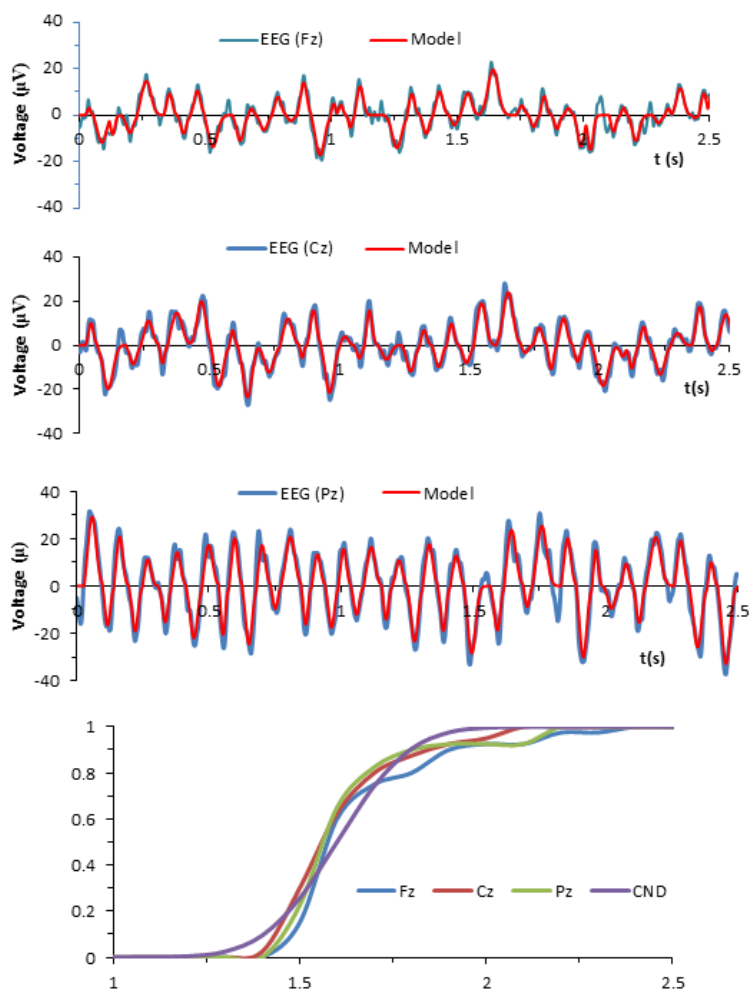


**Figure 6** Upper panels show EEGs from Fz, Cz and Pz recording sites and remarkably accurate models calculated by the method of the HRFD. In the bottom panel the cumulative distribution functions of these processes are compared with the curve of cumulative normal distribution.

The means, standard deviations (SD) and D (K-S statistic) were as follows.

Fz: mean = 1.756 (SD = 0.205), D = 0.106.

Cz: mean = 1.712 (SD = 0.152), D = 0.076.

Pz: mean = 1.721 (SD = 0.182), D = 0.079.

The blue lines in the upper panels show pertinent EEGs from Fz, Cz and Pz cortical sites. The red lines are the models calculated using the HRFD. The bottom panel shows the corresponding cumulative distribution functions normalized by sample size. The line denoted by CND is the cumulative normal distribution.

The greatest discrepancy between the CND and the empirical cumulative distribution, called the D-statistic, serves as a criterion to reject or accept the null hypothesis. Given that all calculated empirical cumulative distributions have been supported by equal numbers of  $\epsilon$  (40 values of  $\epsilon$  employed in the tests), the null hypothesis is rejected if  $D \geq 0.189$  (5%).

The above estimates are well below this value and do not provide any reason to reject the null hypothesis. It is important to note the highly stereotypical character of the test results. The outcomes of multiple tests using the data from subjects from control and patient groups indicate the universality of introduced empirical distributions. Therefore, we can consider HWF an adequate universal model of ERP components.

### 3.1 Conventional and Synthetic Grand Mean ERPs

The analysis of specific features of ERPs in different groups of selected subjects conventionally uses grand mean averages. The left side panels in Figure 7 illustrate grand mean average ERP waveforms calculated by conventional averaging for each group using 40 artefact free single trials from Fz, Cz and Pz middle sites. The histograms in the right-side panels show the elicitation rates of defined components. Taking the total number of single trials as 100%, the bars show the percentages of the sweeps in which components were identified, i.e. the frequencies with which different ERP components appear in single trials.

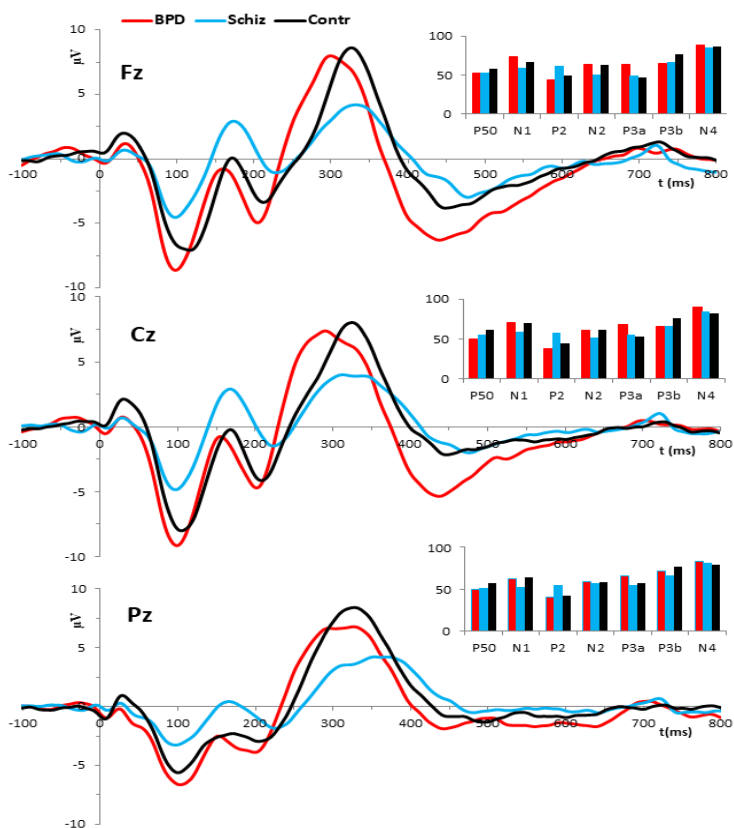


**Figure 7** Grand mean averages obtained by conventional averaging.

One of the most investigated endogenous brain potentials in psychiatric research is the positive ERP wave at approximately 300 ms peak latency range, denoted as P3. This component is clearly seen on all of these records as a monolithic positive waveform with notable broadening of the shape. In all recording sites, the P3s of patients with schizophrenia show a decrease of peak amplitudes. For example, at Cz recording site the 8.03 µV amplitude of the P3 in control subjects is reduced in

patients with schizophrenia to 4.02  $\mu\text{V}$ . Such a trend is consistent with the general consensus that reduced P3 amplitude is one of the most replicable biological observations in schizophrenia [11].

Phenomenologically, it is generally accepted that P3 is created by the coordinated activity of multiple intracranial sources. With regard to the auditory oddball paradigm, there is a good deal of evidence that the P300 elicited by a target stimulus consists of two major components called the P3a and P3b [27].

These are independent and dissociable processes. The main distinguishing feature of the P3a is that it has a significantly shorter latency than P3b the peak latency of which is in the range of 300-400 ms. The morphology of these potentials and their temporal overlap are easily recognizable in typical results of single trial analysis as exemplified in Figure 8.

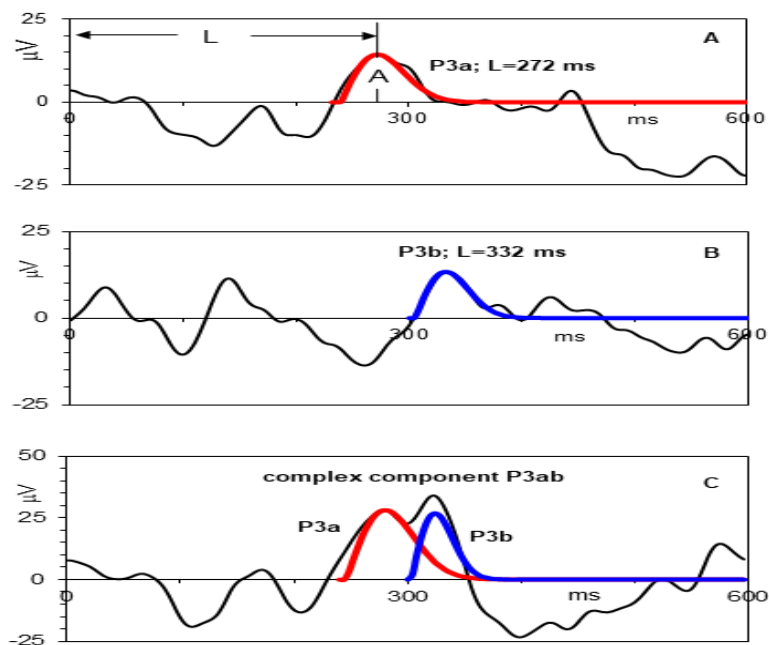


**Figure 8** Various morphologies of the late positive component complex in single trial ERPs recorded in one and the same control subject from the Cz cortical site. The black lines show single trial ERPs induced by target stimuli applied at  $t = 0$ . The colored lines are the models of the P3a and P3b.

However, the capacity of conventional averaging to identify the P3 as a composite of the P3a and P3b components is quite limited. It is particularly demonstrated by Figure 7 where the composite nature of the ERP in the 300 ms range is obscured in conventional averages. For that reason, most previous techniques neglected the existence of the P3a and considered the ERP in the 300 ms range as a single P3(00) component.

By contrast to conventional averaging, the HRFD identifies the whole complex of the late ERP components. Of crucial importance is that this methodology eliminates the temporal overlap of P3a and P3b components, allowing us to treat these ERP components as separate entities with different diagnostic features. The individuality and independence of the P3a and P3b components is supported by our finding that these components comprise 3 major types of activity pattern, both in the control and patient groups. This diversity of ERP patterns in the 300 ms latency range is exemplified in Figure 8. s demonstrates that P3a can occur without P3b and P3b sometimes occurs

without P3a, suggesting the independence of the two waveforms. The third type in panel **C** is a complex component P3ab which develops as the superposition of P3a and P3b produced in one and the same single trial. These data show that there is no basis supporting the assumption of conventional averaging that the P3(00) is a monolithic component with an invariant pattern of activity. These aspects of the variability of ERP components, particularly the co-existence of P3a and P3b components, are obscured in conventional averages.

The HRFD considers a candidate event-related component as being not just a peak in the EEG waveform, but a whole deflection (positive or negative) with a particular shape defined by the set of 3 parameters. After the selection of “true” components using conditions 1-3, the procedure breaks down a single trial ERP into the sum of HWFs which provides a synthetic model of the single trial ERP. The sum of such models for selected components and cortical sites from selected groups of subjects provide synthetic grand mean averages.

Using the same original data as those supporting conventional grand mean averages in Figure 7, the synthetic grand mean ERPs are shown in Figure 9.

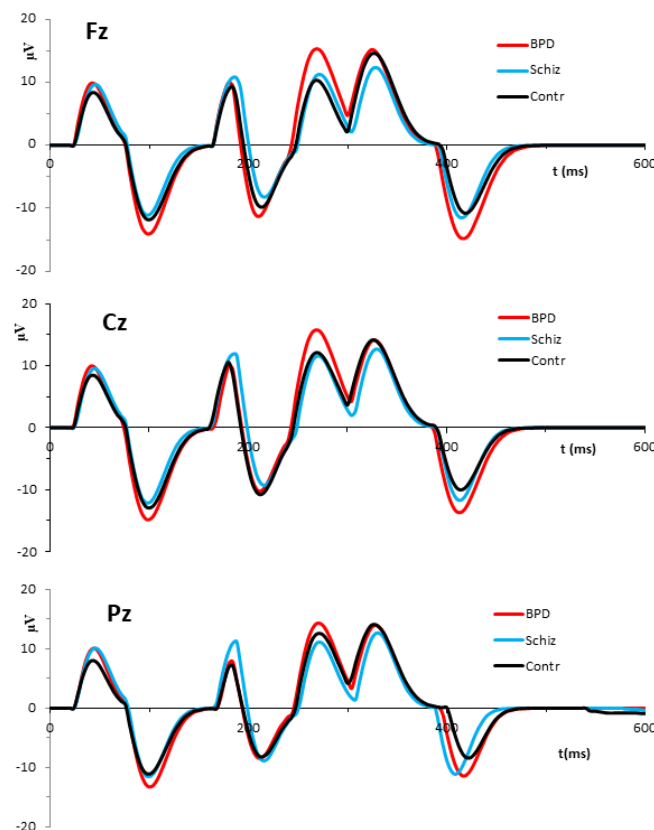


**Figure 9** Synthetic grand mean averages for the same data as in Figure 7.

We see marked differences between the results of the two methods of averaging. Compared with conventional averages, synthetic grand mean averages show significantly increased voltages. This indicates a crucial oversimplification in conventional ensemble averaging which assumes that the ERP components of interest are present in all single trials.

Actually, for the control group the numbers of identified components from the Cz recording site are:  $N_{N1} = 471$ ,  $N_{N2} = 304$ ,  $N_{P2} = 420$ ,  $N_{P3a} = 353$ , and  $N_{P3b} = 505$ , where the subscript is the name of

the component. Given P3b for example, this means that the synthetic average is estimated by the SCA as the sum of 505 identified single trial P3b components divided by an exact number of identified components, i.e. the  $N_{P3b}$ . For the same situation, conventional averaging divides the sum by 680 (i.e. the total number of single trials, 40 single trials for each of 17 subjects).

Another serious problem with conventional averaging is that significant temporal overlap of P3a with P3b creates numerous methodological complications for detection of these components in conventional grand mean averages. This situation is exemplified in Figure 10 which compares the results of conventional (panel A) and selective component averaging (Panel B) using the data from the BPD and control groups.

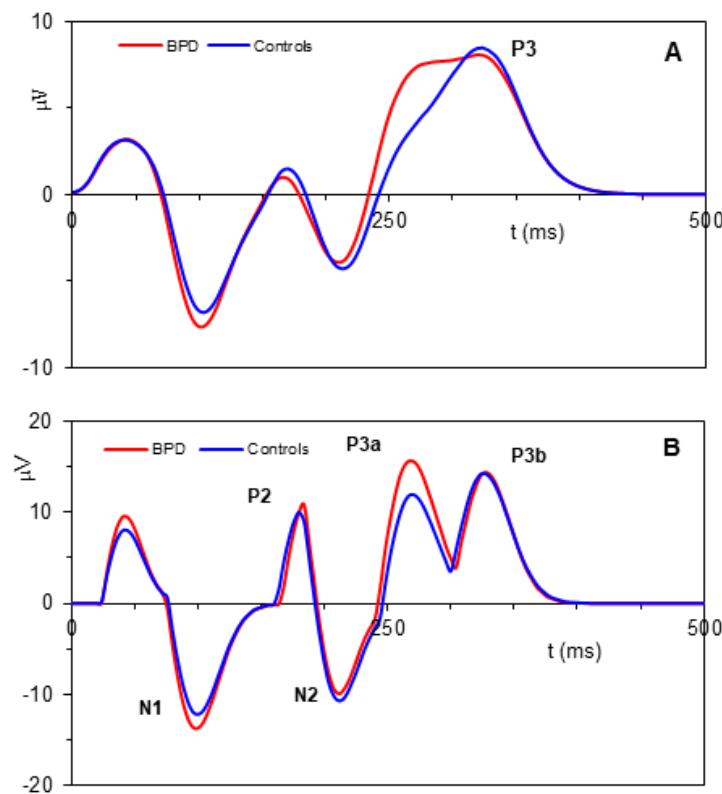


**Figure 10** The panel A illustrates conventional grand mean averages in which P3 appears as a unitary component. By contrast, the synthetic grand mean average in the panel B reveals the P3a-P3b complex components in the 300 ms range.

The ambiguities involved in the interpretation of the ERP parameters from conventional grand mean averages are twofold. The first is that P3a and P3b components remain unknown. Secondly, the variable morphology of these components may affect the amplitude and latency parameters of the P3 from conventional averages in unpredictable ways. Without reliable methods for identifying the composite nature of late components of the ERP, many investigators evaluate complex average waveforms in the 300 ms latency range only for the maximum amplitude and latency, which assumes a monolithic average P3. These methodological difficulties and related simplifications may explain why the P3a has not been observed in ERP studies across different subject and patient populations as consistently as the larger and more prominent P3b.

Reliable recognition of both the P3a and P3b components, unfulfilled by the previous methods, is achieved in our study through creation of a model-based approach to the component identification.

In the following sections we provide evidence that delineation of the P3a-P3b complex, instead of a single P3, has significant potential to enrich the diagnostic power of ERPs. Accordingly, the major focus is on features of P3a and P3b components. The synthetic grand mean averages of these components are shown in Figure 11.

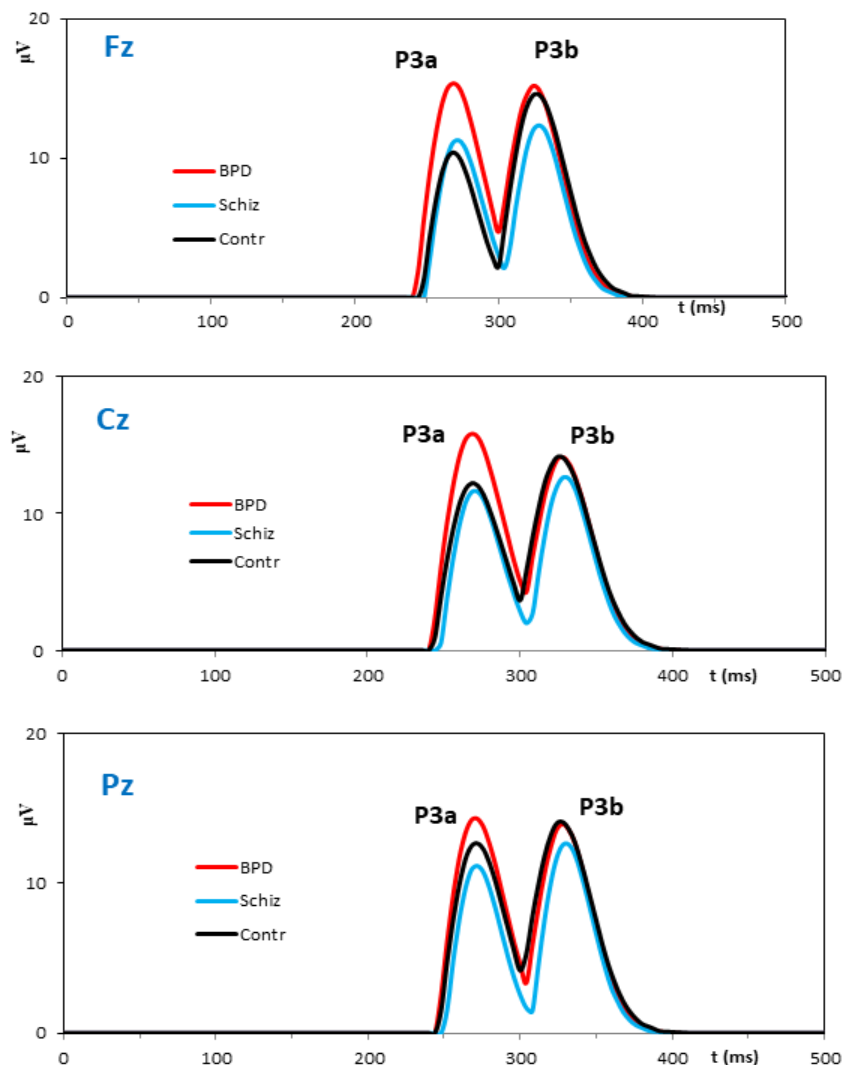


**Figure 11** Grand mean averages of the P3a and P3b components.

The major parameter which defines single trial EEG deflection as a P3a or P3b component is the peak latency. The values of this parameter for middle sites in the 3 groups are listed in the Table 1.

**Table 1** Shows mean latencies and standard deviations (s.d.) in midline electrode sites of subjects from the two patient groups (BPD and schizophrenics) and the group of controls.

		Group 1	Group 2	Group 3	Group comparisons, p	
		BPD	Schizophrenia	Controls	1 vs 3	2 vs 3
ERP	RS	Mean latency (s.d.), ms				
P3a	Fz	269 (0.899)	271 (0.889)	268 (1.01)	Ns	Ns
	Cz	269 (0.801)	270 (0.859)	269 (0.898)	Ns	Ns
	Pz	271 (0.785)	272 (0.896)	271 (0.863)	Ns	Ns
P3b	Fz	326 (0.801)	328 (0.831)	327 (0.682)	Ns	Ns
	Cz	328 (0.761)	330 (0.836)	327 (0.693)	Ns	p < 0.05
	Pz	329 (0.743)	330 (0.807)	328 (0.719)	Ns	p < 0.05

The reason for the closeness in values of peak latencies may be the fact that our methodology of the HRFD eliminates the component overlap which introduces uncontrolled errors in the estimated parameters of average ERPs. The number of trials selected for HRFD can be found in the Table 2 and Table 3. A visual impression of the morphological similarities is demonstrated by the graphs in Figure 11.

**Table 2** Compares the peak amplitudes of the P3a and P3b components for Fz, Cz and Pz recording sites in the subjects from the BPD and control groups. RS denotes recording site and N is the number of single trials selected for HRFD. The A1 and A2 are the peak amplitudes from the BPD and control groups, respectively.

Patients with BPD versus controls						
ERP	RS	N1	A1 (s.d.),	N2	A2 (s.d)	
P3a	Fz	377	15.4 (0.48)	314	10.5(0.35)	p < 0.001
	Cz	437	15.9 (0.45)	353	12.3(0.37)	p < 0.001
	Pz	421	14.5 (0.42)	385	12.8(0.36)	p < 0.01
P3b	Fz	385	14.8 (0.44)	512	14.7(0.34)	Ns
	Cz	426	13.8 (0.39)	505	14.0(0.32)	Ns
	Pz	465	13.7 (0.34)	518	13.9(0.30)	Ns

**Table 3** Comparison of peak amplitudes of P3a and P3b at frontal electrode sites. These sites are illustrated in Figure 12.

Patients with BPD versus controls						
ERP	RS	N1	A1(s.d.)	N2	A2(s.d.)	P
P3a	Fz	377	15.4 (0.48)	314	10.5 (0.35)	p < 0.001
	F3	396	13.6 (0.41)	357	10.0 (0.32)	p < 0.001
	F4	409	14.2 (0.42)	353	10.1 (0.36)	p < 0.001
	F7	373	8.73 (0.26)	424	7.20 (0.19)	p < 0.001
	F8	390	8.90 (0.28)	426	7.14 (0.20)	p < 0.001
P3b	Fz	385	14.8 (0.44)	512	14.7 (0.34)	p > 0.05

F3	400	13.0 (0.35)	519	13.1 (0.30)	p > 0.05
F4	410	13.8 (0.39)	534	13.3 (0.31)	p > 0.05
F7	363	8.11 (0.23)	460	7.91 (0.19)	p > 0.05
F8	356	8.12 (0.26)	474	7.76 (0.22)	p > 0.05

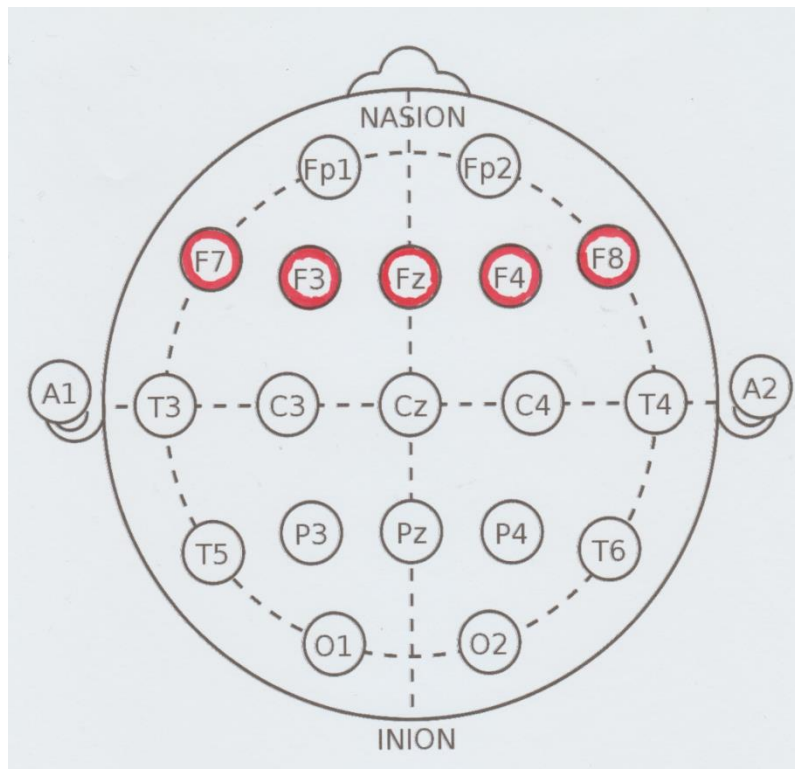


**Figure 12** Topographic map of electrode sites. The circles rendered in red denote the sites of cortical electrodes at which the peak amplitudes of the P3a from the group of BPD patients have shown a statistically highly significant increase of peak amplitudes.

### 3.2 P3a and P3b in BPD Patients Compared with Controls

The data from the Table 1 show that the differences in the peak latencies of P3a and P3b from the group of BPD patients compared with controls are non-significant for all middle recording sites. In contrast, the data from the Table 2 show statistically highly significant increases of P3a peak amplitudes at Fz, Cz and Pz middle sites in BPD patients.

An important feature of these estimates, also evident in Figure 11, is a significant increase of P3a amplitudes in the group of BPD patients. In contrast, estimates of the P3b peak amplitudes didn't reveal significant inter-group changes.

The differences between the values of the P3a peak amplitudes in patient and control groups show increases from Pz to Fz sites. These are: Pz-1.7 (µV), Cz-3.7 (µV), Fz-5.0 (µV).

This trend indicates that the frontal areas of the brain are altered in BPD. Additional support for this tendency is provided by the data in Table 3 with similar comparisons of the peak amplitudes from Fz, F3, F4, F7 and F8 frontal electrode sites.

### 3.3 P3a and P3b in Patients with Schizophrenia

The results of inter-group measurements of the P3a and P3b peak amplitudes in patients with schizophrenia versus controls are presented in Table 4.

**Table 4** Peak amplitudes of P3a and P3b components for Fz, Cz and Pz recording sites in the subjects from the schizophrenia and control groups.

Patients with schizophrenia versus controls						
ERP	RS	N1	A1 (s.d.)	N2	A2 (s.d.)	
P3a	Fz	315	11.4 (0.37)	314	10.5 (0.35)	Ns
	Cz	373	11.8 (0.35)	353	12.3 (0.37)	Ns
	Pz	370	11.3 (0.34)	385	12.8 (0.36)	Ns
P3b	Fz	430	12.3 (0.34)	512	14.7 (0.34)	p < 0.001
	Cz	441	12.7 (0.33)	505	14.0 (0.32)	p < 0.01
	Pz	442	12.7 (0.35)	518	13.9 (0.30)	p < 0.01

RS denotes the recording site. N1 and N2 are the numbers of single trials selected from the group of patients with schizophrenia and controls, respectively. The A1 and A2 are peak amplitudes from schizophrenia and control groups respectively.

The major outcomes are twofold. First, the P3a amplitudes in schizophrenia patients do not show significant changes compared with the data from the group of control subjects. Second, the P3b amplitudes in schizophrenia patients are significantly reduced at all middle electrode sites.

The grand mean averages in Figure 11 give a clear picture of these patterns.

## 4. Discussion

The main findings reported in this paper depend critically on the methodological innovation of EEG and ERP analysis using the probabilistic methods of quantum theories. This novel approach, introduced in earlier papers [5, 6], provides a means of bridging the macro-scale EEG and ERP signals with the underlying molecular events of ion transport at the micro-scale.

We first discuss the micro-scale results, the main aspect of which is the relocation of the models of elementary bioelectric sources of the EEG signal from the cellular to the molecular level. Instead of the continuous time membrane potentials implemented in previous models, the elementary cortical sources of electricity are now allocated to ions, positively and negatively charged particles, the size and stochasticity of which conform in their attributes to quantum mechanics. The vanishingly small role of individual charges in the generation of macroscopic scale EEG signals reduces the problem to the study of the behavior of large numbers of random variables underlying the phenomenon in question. This is realized through the predictions of the central limit theorem.

The idea of EEG interpretation using probabilistic notions was previously put forward by Elul [28]. Based on analysis of the synchronization of EEG sources, Elul proposed that the evolution of brain waves may be governed by statistical regularities following from the central limit theorem. Thus, the EEG waveform may simply be accounted for as a normally distributed output resulting from the combination of the activity of many independent neuronal generators.

This hypothesis has never been supported by an adequate empirically-testable mathematical theory. However, it raised the possibility that “gaussianity” may be the most promising explanatory feature of ERPs. The straight realization of this approach is employment of the normal distribution as a model of N1, P2, N2 and P3 components of average ERPs [29]. One of the major factors that introduce significant inconsistency between the Gaussian function and real ERP waveforms is that normal distribution is a bell-shaped symmetrical function defined on an infinite time scale while the ERP component is a transient process the start of which is locked to the cognitive event with different rates of rise and decay. To take into account a steeply rising left flank and a slowly decreasing right flank the convolution of an exponential and a normal distribution (ex-Gauss function) has been used for quantifying the P3 component in average ERPs [30]. The gamma function is quite flexible and might be one of a variety of possible shapes that fit the component waveforms of average ERPs. However, the ex-Gauss function differs from predictions of the central limit theorem and cannot serve as a universal model of ERP components. In this context, the fundamental point of our approach is consideration of each ERP component as a statistical limit of the underlying microscale processes, the appearance of which, on the global scale, is governed by the central limit theorem. The prediction of this theorem is the normal distribution (the Gaussian function).

A single Gaussian function defined on an infinite scale is not a proper approximation of the ERP component, which is a transient starting from the moment of activation of the underlying cellular machinery by a cognitive event. This feature of ERP components is adequately described in our theory by equation 1 composed of a sum of two shifted Gaussian functions the profile of which appears as an adequate form of the shape of the ERP component. We interpret this paradigm as indicating two ensembles of elementary charges that can be considered as the primary and secondary particle populations.

Physically, cell membranes, which separate intracellular from extracellular space, play a crucial role in the creation of the microscale model. Due to their high electrical resistance, membranes act as a border which prevents intracellular ions from noticeably changing extracellular field potentials. This means that extracellular ions appear to be the source of the global scale EEG and ERP. The impact of a single ion to the field potential is vanishingly small. Therefore, the changes of macroscale potentials are considered as cumulative effects produced by the transport of ions during synchronized activation of ensembles of closely located excitable cells.

In keeping with this, the modelling tools are changed from the deterministic equations of classical physics to the probabilistic formalism of non-homogenous BDPs with time dependent rates of birth and death. This specific amalgamation of deterministic and stochastic factors on the microscopic scale has been called the transient deterministic chaos [6].

We now turn from microscale events to the macroscale phenomena which they produce in the form of EEG and ERP waveforms. The major achievement provided by the methodological innovations of single trial ERP analysis and the creation of synthetic grand mean averages is reliable identification of the P3a and P3b endogenous potentials in the 250-450 latency range. In general, on the basis of conventional averaging, the ERPs in this region have been conceptualized as the P300 arising from a single neural generator. This concept has shaped virtually every aspect of P300 research, including the way it is used in clinical studies. In this context, P300 has been used as an aid to diagnose neuropsychiatric disorders, sub-types of disorder and to evaluate the effects of medication on aspects of cognition. In reference to higher-order cognitive processes, no other

endogenous potential has received as much attention from researchers in the last two decades as the P300. However, converging evidence from a number of experimental and clinical studies has made it evident that significantly different combinations of neural generators contribute to the P300 activity elicited by different combinations of experimental variables. This means that the P300 is not a monolithic component.

The most commonly recognized subcomponent in “oddball” tasks is the classical P3b which has a parietal maximum scalp distribution and a peak latency of 300-400 ms. This is often preceded by a subcomponent, identified as a new component [27]. This component was labeled “P3a”, to distinguish it from the classical Suttonian P300 [31] which was re-labeled “P3b”. These P3 subcomponents usually overlap in time, making it difficult to recognize them in the time course of average ERPs. A specific problem is that ERP waveforms are not measured in single trials and then averaged, but are measured only once, in the average curve. This leads to the loss of crucial information about the morphologies of P3a and P3b components and the rates with which they respond to cognitive stimuli. Hence, the potential for the ERP to provide objective electrophysiological measures of cognitive variables to a large degree depends on our ability to analyze ERP component composition directly from single trial records. Though various filters and templates have been employed, comprehensive single trial ERP analysis has not been achieved using existing methods.

As far as we are aware, our study is the first to provide an empirically testable, adequate model of single trial ERP components. This methodological innovation allows us to eliminate the temporal overlap of P3a and P3b components in single trials and significantly improve the accuracy of the corresponding amplitude and latency parameters. An important and somewhat unexpected finding is the stability of the latencies of both the P3a and P3b components. As the data from the Table 1 indicate, in the control and BPD patient groups the mean peak latency of the P3a at all midline sites is in the range from 268 to 271 ms. For P3b the range is from 326 to 329. For both the P3a and P3b no statistically significant inter-group differences were found.

In schizophrenia patients the inter-group differences in the peak latencies of P3a (the range from 268 to 272 ms) are non-significant. For P3b (the range from 327 to 330 ms), small statistically significant differences in comparison with the control group were documented at Cz and Pz sites.

In contrast to the latency findings, we found profound changes in the peak amplitudes of the P3a and P3b in both patient groups. A critical finding is that there is a qualitatively different character of ERP morphology in the groups of patients with schizophrenia and BPD, suggesting functional differences in the underlying neuropathological processes.

The main distinguishing feature of ERP changes in BPD patients is an abnormal increase of the P3a peak amplitudes compared with control subjects. Table 2 shows a statistically highly significant increase of P3a peak amplitudes at Fz, Cz and Pz middle sites in BPD patients.

The data from Table 3 and Figure 12 demonstrate the frontal origins of this abnormality. Failure of inhibitory control may be the factor that accounts for the missing increase in amplitude of the P3a. In a wider neuro-psychiatric context, our recent aetiological model of BPD suggests that impairment of inhibitory control in prefrontal networks may underlie the disorder [32, 33].

This P3a enlargement gives support to Meares’ hypothesis that the sense of disconnectedness, or disintegration, that is a core phenomenon of BPD, is the outcome of deficient higher order inhibitory function. This hypothesis is based upon a Jacksonian model of dissociation, developed further in current texts on the subject [33, 34].

Our data demonstrate that the main distinguishing feature of ERP changes in patients with schizophrenia is an abnormal decrease of the peak amplitudes of P3b, while the voltage of P3a is not affected by this pathology. The reduction in amplitude of the average P3 from the standard auditory oddball paradigm is one of the most replicable biological observations of schizophrenia, present regardless of medication status [11].

Our study indicates that the voltage reduction of the average P3 depends on two factors. The first factor is a replication of previous analyses, where the voltage reduction of P3 components is identified in single trials. This indicates a reduced impact of microscale sources on the macroscale P3. A second factor, newly identified in this study, is the demonstration of a decreased number of single trials which contain the P3b component.

The techniques of single trial ERP analysis employed in previous studies were limited in terms of capturing the P3a and P3b sub-components of the P3. The investigation of spatiotemporal distributions of single trial P3a and P3b using the methodological innovation of HRFD suggests a distinct character of these components. The major properties of the average P3 resemble single trial P3b. However, the temporal overlap of the P3a and P3b components and their changing patterns from trial-to-trial cause unpredictable changes of the latency and amplitude parameters of average P3s.

The P3a has been studied in patients with schizophrenia much less frequently than P3b. Usually, lower or unchanged amplitudes of P3a have been described in schizophrenia [35]. Consistent with these findings, our study did not reveal significant changes in the voltages of P3a in schizophrenia.

A main inference from these results is that BPD and schizophrenia are physiologically different. Since they are disorders which have in common the identifying feature of disconnectedness, it is sometimes argued that they are the same. However, this study demonstrates an abnormality of P3a which is clearly defined in BPD but absent in schizophrenia.

## **5. Conclusions**

In this study we have applied original methods of quantum and component signal analysis, introduced previously [5, 6], allowing advanced ERP analysis, which has created an opportunity for the development of remarkably accurate models of ERP waveforms directly from single trial recordings. These solutions are of great significance, because they provide additional information about the organization of cognitive processes within the individual, demonstrating specific disturbances of information processing. Given that the P300 is seen as a robust marker of psychiatric disorders, these novel illustrations of single trial recordings constitute evidence that demands reconsideration of the old concept of P300 as an ERP component arising from a single neural generator. Our methodology indicates that significantly different combinations of neural generators contribute to the P300 activity elicited by different experimental variables. In the studied subject groups, the P3a and P3b have both been identified as major components of P300. This improved recognition of patterns in the electrophysiological data enables differentiation of borderline personality disorder from schizophrenia. The methodology is universal and can be applied to different types of ERPs. A basic limitation, which in the relaxed state is unlikely to present difficulties, is that the muscular components of recorded potentials need to be significantly lower than the potentials produced from neuronal sources.

## Author Contributions

Dr. Melkonian, Dr. Korner, Prof. Meares and Prof. Harris conceptualized the work and manuscript. Dr. Korner was accepted as responsible for project development. Dr. Melkonian supported the methodology by the algorithms and software using which the data analysis and interpretation was performed. Prof. Meares provided the data from the group of patients with BPD and interpreted the results in terms of his Jacksonian model of dissociation. Prof. Harris provided spectral analysis findings from the group of patients with schizophrenia and the control group. Dr. Melkonian wrote the original draft. Dr. Korner provided review and editing.

## Competing Interests

The authors have declared that no competing interests exist.

## References

1. Donchin E, Ritter W, McCallum WC. Cognitive psychophysiology: The endogenous components of the ERP. Event-related brain potentials in man. New York: Academic Press; 1978.
2. Avitan L, Teicher M, Abeles M. EEG generator—a model of potentials in a volume conductor. *J Neurophysiol.* 2009; 102: 3046-3059.
3. Buzsáki G, Anastassiou CA, Koch C. The origin of extracellular fields and currents—EEG, ECoG, LFP and spikes. *Nat Rev Neurosci.* 2012; 13: 407-420.
4. Cohen MX. Where does EEG come from and what does it mean? *Trends Neurosci.* 2017; 40: 208-218.
5. Melkonian D, Blumenthal T, Barin E. Quantum theory of mass potentials. *PLoS One.* 2018; 13: e0198929.
6. Melkonian D. Quantum theory of EEG with application to the single-trial ERP analysis. *OBM Neurobiol.* 2021; 5: 084.
7. Kozłowska K, Melkonian D, Spooner CJ, Scher S, Meares R. Cortical arousal in children and adolescents with functional neurological symptoms during the auditory oddball task. *NeuroImage.* 2017; 13: 228-236.
8. Meares R, Melkonian D, Gordon E, Williams L. Distinct pattern of P3a event-related potential in borderline personality disorder. *Neuroreport.* 2005; 16: 289-293.
9. Meares R, Stevenson J, Gordon E. A Jacksonian and biopsychosocial hypothesis concerning borderline and related phenomena. *Aust N Z J Psychiatry.* 1999; 33: 831-840.
10. Yee L, Korner AJ, McSwiggan S, Meares RA, Stevenson J. Persistent hallucinosis in borderline personality disorder. *Compr Psychiatry.* 2005; 46: 147-154.
11. Ford JM, White P, Lim KO, Pfefferbaum A. Schizophrenics have fewer and smaller P300s: A single-trial analysis. *Biol Psychiatry.* 1994; 35: 96-103.
12. Kutchera SP, Blackwood DH, Gaskell DF, Muir WJ, Clair DS. Auditory P300 does not differentiate borderline personality disorder from schizotypal personality disorder. *Biol Psychiatry.* 1989; 26: 766-774.
13. Neher E, Sakmann B. Single-channel currents recorded from membrane of denervated frog muscle fibres. *Nature.* 1976; 260: 799-802.
14. Freeman WJ. Mass action in the nervous system. New York: Academic Press; 1975.

15. Plonsey R. Bioelectric phenomena. New York, NY: McGraw-Hill; 1969.
16. Melkonian D. Mathematical theory of chemical synaptic transmission. *Biol Cybern.* 1990; 62: 539-548.
17. Melkonian D. Transient analysis of a chemical synaptic transmission. *Biol Cybern.* 1993; 68:341-350.
18. Gnedenko BV, Kolmogorov AN. Limit distributions for sums of independent random variables. Boston, MA: Addison-Wesley Publishing Company; 1954.
19. Bekefi G, Barrett A. Electromagnetic vibrations, waves, and radiation. Cambridge: MIT Press; 1977.
20. Melkonian D, Gordon E, Bahramali H. Single-event-related potential analysis by means of fragmentary decomposition. *Biol Cybern.* 2001; 85: 219-229.
21. Melkonian D, Blumenthal T, Gordon E. Numerical Fourier transform spectroscopy of EMG half-waves: Fragmentary-decomposition-based approach to nonstationary signal analysis. *Biol Cybern.* 1999; 81: 457-467.
22. Melkonian D, Blumenthal TD, Meares R. High-resolution fragmentary decomposition—a model-based method of non-stationary electrophysiological signal analysis. *J Neurosci Methods.* 2003; 131: 149-159.
23. Melkonian D. Similar basis function algorithm for numerical estimation of Fourier integrals. *Numer Algorithms.* 2010; 54: 73-100.
24. Harris A, Melkonian D, Williams L, Gordon E. Dynamic spectral analysis findings in first episode and chronic schizophrenia. *Int J Neurosci.* 2006; 116: 223-246.
25. American Psychiatric Association (APA) Diagnostic and statistical manual of mental disorders. 4th ed. Washington DC: American Psychiatric Association; 1994.
26. Blom JL, Anneveldt M. An electrode cap tested. *Electroencephalogr Clin Neurophysiol.* 1982; 54: 591-594.
27. Squires NK, Squires KC, Hillyard SA. Two varieties of long-latency positive waves evoked by unpredictable auditory stimuli in man. *Electroencephalogr Clin Neurophysiol.* 1975; 38: 387-401.
28. Elul R. Brain waves: Intracellular recordings and statistical analysis help clarify their physiological significance. In: *Data acquisition and processing in biology and medicine.* Oxford: Pergamon press; 1966.
29. Haig AR, Rennie C, Gordon E. The use of Gaussian component modelling to elucidate average ERP component overlap in schizophrenia. *J Psychophysiol.* 1997; 11: 173-187.
30. Verleger R, Wascher E. Fitting ex-Gauss functions to P3 waveshapes: An attempt at distinguishing between real and apparent changes of P3 latency. *J Psychophysiol.* 1995; 9: 146-158.
31. Sutton S, Tueting P, Zubin J, John ER. Information delivery and the sensory evoked potential. *Science.* 1967; 155: 1436-1439.
32. Meares R. The contribution of Hughlings Jackson to an understanding of dissociation. *Am J Psychiatry.* 1999; 156: 1850-1855.
33. Meares R. *Dissociation model of borderline personality disorder.* New York: WW Norton & Company; 2012.
34. Farina B, Meares R. The traumatic disintegration dimension. In: *Dissociation and the dissociative disorders: Past, present, future.* New York & London: Routledge; 2022.
35. Kruiper C, Fagerlund B, Nielsen MØ, Düring S, Jensen MH, Ebdrup BH, et al. Associations

between P3a and P3b amplitudes and cognition in antipsychotic-naïve first-episode schizophrenia patients. *Psychol Med.* 2019; 49: 868-875.